

Low-temperature expansions for the step free energy and facet shape of the simple-cubic Ising model

Mark Holzer and Michael Wortis

Department of Physics, Simon Fraser University, Burnaby, British Columbia, Canada V5A 1S6

(Received 12 July 1989)

We report here the first systematic low-temperature expansion of the step free energy for the simple-cubic nearest-neighbor Ising model and we obtain the facet shapes for the associated equilibrium crystal-shape problem. An expansion scheme is developed which makes explicit use of the conjugacy between the step free energy and the facet shape. The calculation is structured as a perturbation expansion about the exact solution for the interfacial free energy of the two-dimensional square Ising model. We find that the facet shape is approximated to better than 1% by the equilibrium crystal shape of the two-dimensional Ising model for temperatures less than about 72% of the roughening temperature. In that temperature range overhangs and bubbles contribute less than 0.1% to the step free energy. At higher temperatures the facet shape is nearly circular with anisotropies of less than 0.4% and a ratio of facet diameter to crystal diameter of less than 0.4. Extrapolations into the isotropic region give critical roughening amplitudes consistent with recent Monte Carlo data.

I. INTRODUCTION

The physics of the solid-fluid interface has been an active field of condensed-matter research in recent years. In particular, the roughening transition and equilibrium crystal shapes have received much attention and have been reviewed by several authors.¹⁻⁴ One of the most basic quantities characterizing such an interface is the anisotropic step free energy $\gamma(\theta)$, the excess free energy associated with the creation of a unit length of a single step, oriented at average angle θ with respect to the surface crystal axes, on an otherwise macroscopically flat surface.⁵ Exact solutions for $\gamma(\theta)$ exist for restricted solid-on-solid (RSOS) models isomorphic to the six-vertex model.⁶⁻⁸ While these models show the expected universal XY-dual behavior at the roughening transition,⁹ they suffer from being unrealistic. The RSOS condition has the shortcoming of suppressing many excitations isoenergetic with those included. Such excitations, although irrelevant in a renormalization-group sense,¹⁰ will nonetheless alter the detailed, nonuniversal temperature evolution of $\gamma(\theta)$. An analytical calculation of $\gamma(\theta)$ for a more realistic model has so far not been performed.

In this paper we present the first systematic low-temperature (T) expansion of the step free energy for the simple-cubic (SC) nearest-neighbor Ising model. Our emphasis here will be on the connection between the step free energy and the shape of the corresponding facet of the associated equilibrium-crystal-shape (ECS) problem. As pointed out in Refs. 3 and 11, the step free energy and facet shape are related via a Legendre transform, provided that the ECS has no slope discontinuity at the facet edge. Making explicit use of this fact, we develop two expansions, one directly for the step free energy $\gamma(\theta)$ (canonical) and one for the facet shape $y(x)$ (grand canonical). The expansion for $\gamma(\theta)$ about its $T=0$ cusps

is divergent where the expansion of $y(x)$ is perfectly well behaved, and in that sense the two expansions complement each other.

We focus on the SC Ising model not only because of its simplicity and its fundamental importance to statistical mechanics but also because it allows us to make contact with the work of others. In addition to recent Monte Carlo data¹² for $\gamma(\theta=0)$, low-temperature expansions by Weeks *et al.*^{13,14} for the (100) facet of SC Ising and the associated SOS model allow the determination of the corresponding surface tensions $\Gamma(100)$ (Ref. 15) and roughening temperatures T_R (Ref. 16). The expansions of Weeks *et al.* involve the combinatorics of finite clusters of adsorbed and/or desorbed atoms on an otherwise flat interface. In this work, we are faced with the more difficult problem of counting the configurations available to these excitations in the presence of a step running across the interface. Because of their interactions with the step and the many degrees of freedom of the step itself, the complete combinatorics becomes exceedingly involved. Fortunately, however, a large subset of configurations is in one-to-one correspondence with those of the two-dimensional (2D) Ising equilibrium-crystal-shape problem, for which an exact solution is known.¹⁷⁻¹⁹ We exploit this fact by structuring the expansions accordingly. While this simplifies our problem considerably, the remaining combinatorics is still non-trivial.

We generate fifth- and eleventh-order series for $\gamma(\theta)$ and $y(x)$, respectively. We estimate convergence of these series for the symmetry directions to be better than 1% for $T < 0.78T_R$. Normalizing the step free energy to the surface free energy of the facet, we calculate the ratio of the facet diameter to the (100) diameter of the crystal. Below $0.72T_R$ we find that the facet shape is given to better than 1% by the 2D Ising ECS. Corrections due to

overhangs and bubbles contribute less than 0.1% in this temperature region. Above $0.72T_R$ the facet shape is essentially circular. From numerical extrapolations into the critical region we obtain estimates for the roughening temperature and for the critical amplitudes.

The remainder of this paper is organized as follows: In Sec. II we give the conceptual framework on which our expansions are founded. The Legendre-transform conjugacy between the step free energy and the facet shape is derived, and we show that the facet may be thought of as a 2D ECS. We obtain expressions for the step free energy and facet shape in terms of a canonical and grand canonical partition function, respectively. In Sec. III we use the formalism of the previous section to calculate the step free energy and the shape of the (100) facet of the SC Ising model. In Sec. IV convergence estimates for the low-temperature series are developed. The feasibility of extracting critical parameters from the series is discussed. The results of such extrapolations are shown to be consistent with Monte Carlo estimates. We conclude in Sec. V.

II. STEP FREE ENERGIES AND FACET SHAPES FROM INTERFACIAL FREE ENERGIES AND EQUILIBRIUM CRYSTAL SHAPES

Consider a system of total volume V in equilibrium at a first-order phase boundary. To keep the discussion simple, we shall tacitly assume the two phases to be symmetric, as they are in the Ising model.²⁰ Let $\mathcal{H}_{\hat{\mathbf{m}}}$ denote the Hamiltonian of this system, when the two phases are forced to coexist separated by a macroscopically planar interface of surface normal $\hat{\mathbf{m}}$ and area A (Ref. 21). When the system consists of only one phase, we denote the corresponding Hamiltonian by \mathcal{H}_0 . The interfacial free energy per unit area $\Gamma(\hat{\mathbf{m}})$ (surface tension) is defined as the difference between the free energy of the system with and without the interface,

$$\Gamma(\hat{\mathbf{m}}) = -k_B T \lim_{A \rightarrow \infty} \frac{1}{A} (\ln \text{Tre}^{-\beta \mathcal{H}_{\hat{\mathbf{m}}}^{\wedge}} - \ln \text{Tre}^{-\beta \mathcal{H}_0}), \quad (1a)$$

or equivalently

$$\Gamma(\hat{\mathbf{m}}) = \lim_{A \rightarrow \infty} \frac{1}{A} (-k_B T \ln \text{Tre}^{-\beta \mathcal{H}_{\hat{\mathbf{m}}}^{\wedge}} - V f_b), \quad (1b)$$

where k_B is Boltzmann's constant, $\beta \equiv (k_B T)^{-1}$, and

$$f_b = -k_B T \lim_{V \rightarrow \infty} [(1/V) \ln \text{Tr} \exp(-\beta \mathcal{H}_0)]$$

$$\tilde{f}(\boldsymbol{\eta}) = \lim_{A_{xy} \rightarrow \infty} \frac{1}{A_{xy}} \left\{ -k_B T \ln \sum_{\{\hat{\mathbf{m}}\}} \text{Tr} \exp \left[-\beta \left[\mathcal{H}_{\{\hat{\mathbf{m}}\}} + \boldsymbol{\eta} \cdot \int_{\mathcal{S}} (m_x, m_y) d\mathcal{S} \right] - V f_b \right] \right\}, \quad (6)$$

where $A_{xy} \equiv A / (1 + \mathbf{p}^2)^{1/2}$, \mathcal{S} is the microscopic surface separating the two phases, $\hat{\mathbf{m}} = (m_x, m_y, m_z)$ is the local normal of \mathcal{S} , $\mathcal{H}_{\{\hat{\mathbf{m}}\}}$ is the Hamiltonian²⁶ of the system for which an arbitrary macroscopic interface has been enforced (of planar topology but not necessary globally planar), and $\sum_{\{\hat{\mathbf{m}}\}}$ sums over all such systems possible. In

is the bulk free energy per unit volume. These thermodynamic limits exist if microscopic interactions are sufficiently short ranged.^{20,21} Once $\Gamma(\hat{\mathbf{m}})$ is known, the ECS is determined by thermodynamics: In equilibrium the total interface free energy must be minimized, subject to the constraint that the subvolume enclosed by the interface remain fixed. An elegant geometrical solution of this problem is provided by the Wulff construction,^{22,23} which asserts that the ECS is, to within an overall scale λ , the interior envelope of the family of planes perpendicular to and through the points $\hat{\mathbf{m}}\Gamma(\hat{\mathbf{m}})$ (the "Wulff plot"). If we describe the ECS in Cartesian coordinates as $z = z(\mathbf{x})$, $\mathbf{x} = (x, y)$, the analytical statement of the Wulff construction takes on a particularly transparent form: If we let

$$f(\mathbf{p}) = \Gamma(\hat{\mathbf{m}})(1 + \mathbf{p}^2)^{1/2} \quad \text{with } \mathbf{p} = \frac{\partial z}{\partial \mathbf{x}}$$

and

$$\hat{\mathbf{m}} = (-p_x, -p_y, 1) / (1 + \mathbf{p}^2)^{1/2}, \quad (2)$$

the normalized ECS is given by²⁴

$$z(\mathbf{x}) = \frac{1}{\lambda} \tilde{f}(-\lambda \mathbf{x}), \quad (3)$$

where $f(\mathbf{p})$ and $\tilde{f}(\boldsymbol{\eta})$ are related through the Legendre transform

$$\tilde{f}(\boldsymbol{\eta}) = f(\mathbf{p}) - \boldsymbol{\eta} \cdot \mathbf{p}. \quad (4)$$

$\boldsymbol{\eta}$ and \mathbf{p} are conjugate variables related by

$$\boldsymbol{\eta} = \frac{\partial f(\mathbf{p})}{\partial \mathbf{p}} \quad (5a)$$

and

$$\mathbf{p} = - \frac{\partial \tilde{f}(\boldsymbol{\eta})}{\partial \boldsymbol{\eta}}. \quad (5b)$$

The constant λ is the Lagrange multiplier of the constant volume constraint and related to the pressure difference between the two phases.²⁵ λ sets the overall length scale of the ECS.

At this point it is very useful to note that, in going from $f(\mathbf{p})$ to $\tilde{f}(\boldsymbol{\eta})$ [Eq. (4)], we have passed from a "canonical" ensemble at fixed macroscopic slope \mathbf{p} to a "grand canonical" ensemble, where all \mathbf{p} are allowed and $\boldsymbol{\eta}$ (the external-field variable) selects a slope \mathbf{p} (the magnetization or density variable) according to (5b). \tilde{f} may thus be written as^{4,8}

SOS models, the microscopic interface is simply connected and single valued so that

$$\boldsymbol{\eta} \cdot \int_{\mathcal{S}} (m_x, m_y) d\mathcal{S} = -\boldsymbol{\eta} \cdot \int_{A_{xy}} \boldsymbol{\mathcal{A}}(\mathbf{x}) dx dy,$$

where $\boldsymbol{\mathcal{A}}(\mathbf{x})$ is the microscopic slope of the interface.^{4,8,14}

Facets in the ECS arise from cusps of the Wulff plot

$\hat{\mathbf{m}}\Gamma(\hat{\mathbf{m}})$. In order for a cusp (which we take to be at $\hat{\mathbf{m}}_f = \hat{\mathbf{z}}$) to correspond to a facet with a smooth edge, it must be of the form²⁷

$$\Gamma(\hat{\mathbf{m}}) = \Gamma(\hat{\mathbf{z}}) + \frac{\gamma(\theta)}{a}\phi + \alpha(\theta)\phi^v + \dots \quad (7a)$$

with

$$\frac{\gamma(\theta)}{a} \equiv \lim_{\phi \rightarrow 0} \left. \frac{\partial \Gamma}{\partial \phi} \right|_{\theta}, \quad (7b)$$

where $v > 1$ and θ and ϕ are the usual polar angles.²⁸ The physical content of the right-hand side (rhs) of (7b), which allows its identification with $\gamma(\theta)/a$ and forms the basis of our canonical expansion for $\gamma(\theta)$, may be seen as follows: Consider a vicinal surface, that is, an interface whose surface normal $\hat{\mathbf{m}} = \hat{\mathbf{z}} + \delta\hat{\mathbf{m}}$, with $\delta\hat{\mathbf{m}} = \delta\phi(\sin\theta, \cos\theta, 0)$. Microscopically, this interface consists of steps of height a which, on average, are inclined at angle θ with respect to the $\hat{\mathbf{x}}$ axis, are parallel, and are separated by a distance $l \gg a$ so that $\delta\phi = a/l$. Consider a patch of this interface of area $A = lL$ including a net length of step L . The rhs of (7b) then reads by definition [Eq. (1)]

$$\lim_{\phi \rightarrow 0} \left. \frac{\partial \Gamma}{\partial \phi} \right|_{\theta} = -k_B T \lim_{l \rightarrow \infty} \frac{1}{a} \lim_{L \rightarrow \infty} \frac{1}{LL} (\ln \text{Tre}^{-\beta \mathcal{H}_{z+\delta\hat{\mathbf{m}}}} - \ln \text{Tre}^{-\beta \mathcal{H}_{\hat{\mathbf{z}}}}) \quad (8a)$$

$$= \frac{1}{a} \lim_{L \rightarrow \infty} \frac{1}{L} \left[-k_B T \ln \text{Tre}^{-\beta \mathcal{H}_{z,\theta}} - A \Gamma(\hat{\mathbf{z}}) - V f_b \right] \equiv \frac{\gamma(\theta)}{a}, \quad (8b)$$

where $\mathcal{H}_{z,\theta}$ denotes the Hamiltonian for a system with a single step of orientation θ running across the facet of normal $\hat{\mathbf{z}}$. Equation (8b) will be the starting point for our canonical expansion scheme for $\gamma(\theta)$. It emphasizes that the step free energy is defined in precise analogy to the interfacial free energy [Eq. (1)].

A simple but important consequence of the linear cusp (7) is that the 3D Wulff construction for the ECS contains a 2D Wulff construction for the facet shape.^{3,11} To see this, consider a cut through the 3D Wulff construction at fixed θ (see Fig. 1). It follows from elementary geometry that, in the plane of this cut and in the limit as $\phi \rightarrow 0$, the intersection of the Wulff plane belonging to $\hat{\mathbf{m}}(\theta, \phi)$ (the edge plane) with the Wulff plane of the cusp (the facet plane) occurs at $\gamma(\theta)/a$. The line of intersection of the edge plane with the facet plane is, therefore, at a perpendicular distance $\gamma(\theta)/a$ from the cusp. Carrying out this procedure for every angle θ produces a family of lines in the facet plane, each member of which is at perpendicular distance $\gamma(\theta)/a$ from the cusp. The facet shape is the interior envelope of these lines because the ECS is the interior envelope of the corresponding planes. This shows explicitly that the facet shape is obtained as the 2D Wulff construction of a polar plot of $\gamma(\theta)/a$. It is straightforward to show that, wherever $\gamma(\theta)$ is differentiable, the

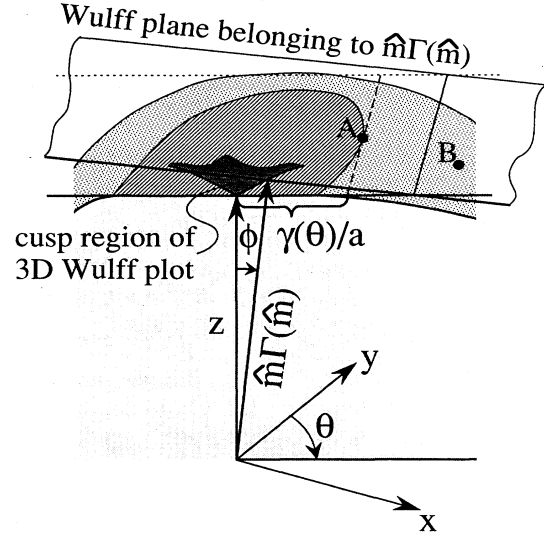


FIG. 1. Perspective view of a fixed- θ cut through the ECS and its Wulff plane as described in the text. The Wulff plane shown is tangent to the ECS at point B in the rounded or rough region of the ECS. In the limit as $\phi \rightarrow 0$ ($\hat{\mathbf{m}} \rightarrow \hat{\mathbf{z}}$) this plane intersects the facet plane, which is the Wulff plane of the cusp, along a line (dashed) which is at perpendicular distance $\gamma(\theta)/a$ from the cusp and tangent to the facet at point A . The facet shape is obtained as the 2D Wulff construction of $\gamma(\theta)/a$.

Cartesian coordinates of the facet shape $\mathbf{x}_f = (x_f, y_f)$ are given by

$$\begin{aligned} x_f &= \frac{1}{\lambda a} \left[\gamma(\theta) \sin\theta + \frac{\partial \gamma(\theta)}{\partial \theta} \cos\theta \right], \\ y_f &= \frac{1}{\lambda a} \left[\gamma(\theta) \cos\theta - \frac{\partial \gamma(\theta)}{\partial \theta} \sin\theta \right], \end{aligned} \quad (9)$$

which gives the facet outline parametrically in terms of θ (Ref. 29). The shape of the facet outline is solely determined by $\gamma(\theta)$. The fact that the facet shape is given by a 2D Wulff construction based on the step free energy $\gamma(\theta)$ has a simple physical explanation: Adjacent to the facet edge, the slope of the rounded region approaches the zero, so steps become widely separated in the thermodynamic limit. Thus, the edge of the facet may be regarded microscopically as a single step encircling the (macroscopically) planar facet region. The minimum-free-energy configuration of this step is given by the 2D Wulff construction.

To make it algebraically manifest that Eq. (9) indeed expresses \mathbf{x}_f as the Legendre transform of $\gamma(\theta)$, we define

$$f(s) \equiv \frac{\gamma(\theta)}{\lambda a} (1+s^2)^{1/2}, \quad (10)$$

with $s \equiv -\partial y_f / \partial x_f = \tan\theta$. Then (9) may be expressed as

$$y_f(x_f) = f(s) - x_f s, \quad x_f = \frac{\partial f}{\partial s}, \quad s = -\frac{\partial y_f}{\partial x_f}. \quad (11)$$

We may, therefore, write

$$y_f(x_f) = \frac{1}{\lambda a} \lim_{L_x \rightarrow \infty} \frac{1}{L_x} \left[-k_B T \ln \sum_{\theta} \text{Tre}^{-\beta[\mathcal{H}_{z,\theta} - \lambda a x_f \hat{x} \cdot \int_{\mathcal{L}} \hat{d}\mathcal{L}] - A \Gamma(\hat{z}) - V f_b} \right], \quad (12)$$

where $L_x = L/(1+s^2)^{1/2}$, \mathcal{L} is the line representing the microscopic step (see Fig. 2 and below), \hat{z} is the (2D) normal of \mathcal{L} , and \sum_{θ} sums over systems with all possible macroscopic step orientations θ . Equation (12) will form the basis of our grand canonical series expansion for $y_f(x_f)$.

To elucidate the physical content of Eq. (12), it is useful to derive it directly from the grand canonical formulation of the ECS. If we define $\eta_f \equiv -\lambda x_f$, then Eqs. (4) and (6) give x_f implicitly as the solution to

$$\lim_{\eta \rightarrow \eta_f} \lim_{A_{xy} \rightarrow \infty} \frac{1}{A_{xy}} \left[-k_B T \ln \sum_{\{\hat{m}\}} \text{Tre}^{-\beta[\mathcal{H}_{\{\hat{m}\}} + \eta \cdot \int_{\mathcal{S}} (\Delta m_x, \Delta m_y) d\mathcal{S}] - A_{xy} \Gamma(\hat{z}) - V f_b} \right] = 0, \quad (13)$$

where $\Delta \hat{m} \equiv \hat{m} - \hat{z}$. While the sum in (13) extends over systems with all possible interface configurations, only those with vicinal surfaces contribute in the limit $\eta \rightarrow \eta_f$. We can, therefore, restrict the ensemble to the subspace of systems which have a single step running across the facet of interest, i.e., we take $\sum_{\{\hat{m}\}} \rightarrow \sum_{\theta}$ and $\mathcal{H}_{\{\hat{m}\}} \rightarrow \mathcal{H}_{z,\theta}$. A strip of the interface of such a system of width L_x is shown in Fig. 2, projected onto the xy plane. $\Delta \hat{m} = 0$ everywhere on the interface except on the "cliffs" of height a (represented by lines in the figure). We may, therefore, write for the field term of Eq. (13)

$$\begin{aligned} \eta \cdot \int_{\mathcal{S}} (\Delta m_x, \Delta m_y) d\mathcal{S} &= a \eta \cdot \int_{\mathcal{L}} d\mathcal{L} \hat{z} \\ &= a \eta_y L_x + a \eta_x \hat{x} \cdot \int_{\mathcal{L}} d\mathcal{L} \hat{z}, \end{aligned} \quad (14)$$

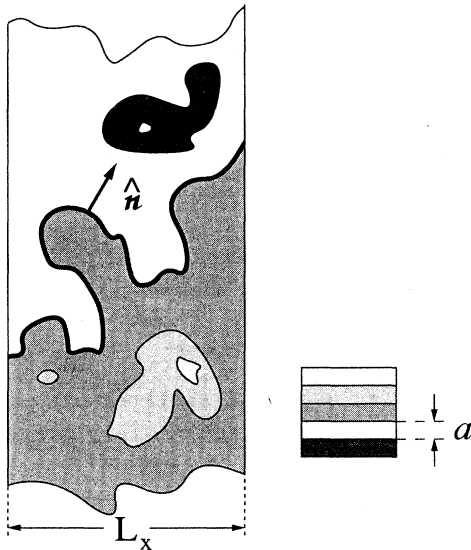


FIG. 2. A strip of vicinal surface projected onto the xy plane. The shading represents lattice planes of spacing a at different levels. The strip contains a "bare" step \mathcal{L} (bold line) and excitations on the terraces to either side of the step (closed curves). \hat{n} is the 2D microscopic normal to the step in the xy plane. The field contribution to the grand canonical Hamiltonian $\eta \cdot \int_{\mathcal{S}} (\Delta m_x, \Delta m_y) d\mathcal{S} = a \eta \cdot \int_{\text{all curves}} d\mathcal{L} \hat{z}$ vanishes around closed curves and therefore couples only to the "bare" step.

where we have taken advantage of the fact that these integrals vanish when taken around closed islands. Substituting this into (13) and noting that the η_y term is independent of step configuration establishes (12) without any direct reference to $\gamma(\theta)$.

Equations (9) and (12) give the size of the facet at given λ . Experimentally, however, we would like to know the coordinates of the facet relative to the physical size of the crystal. As a theoretically convenient and experimentally well-defined measure of the crystal size, we take the center-of-crystal to center-of-facet distance, which is simply $\Gamma(\hat{m}_f)/\lambda$ [cf. Eq. (3)]. The relative facet coordinates (ξ_f, η_f) are, therefore, given by

$$(\xi_f, \eta_f) = \frac{\lambda}{\Gamma(\hat{m}_f)} (x_f, y_f). \quad (15)$$

Finally, we remark that, for some intervals of θ , the facet plane may be discontinuously truncated by Wulff planes from a part of the Wulff plot distant from the facet's cusp. For such θ , vicinal planes are thermodynamically unstable and $\gamma(\theta)$ does not exist. Where $\gamma(\theta)$ does exist, the corresponding facet shape is (for short-ranged forces) smooth for all $0 < T < T_R$, because the step is essentially a 1D object and can have phase transitions [i.e., cusps in $\gamma(\theta)$] at $T=0$ only. We now turn to the problem of calculating explicitly low-temperature expansions for the step free energy and facet shape of the SC Ising model.

III. LOW-TEMPERATURE SERIES FOR THE SIMPLE-CUBIC ISING MODEL

The Hamiltonian of the nearest-neighbor (NN) SC Ising model is

$$\mathcal{H} = -J \sum_{\langle \text{NN} \rangle} \sigma_i \sigma_j, \quad (16)$$

where the "spins" $\sigma_j = \pm 1$ are located at the vertices of a simple-cubic lattice of lattice constant a and the sum is over nearest-neighbor pairs. To keep our equations uncluttered in the remainder of this paper, we shall set the overall scale factor $\lambda a^3/J = 1$ and measure lengths in units of a , temperature in units of J/k_B , and energy in units of J . (We shall also drop the subscripts on x_f and y_f from here on.) In the lattice-gas interpretation of (16), $\sigma_j = +1$ means site j is occupied (by an "atom");

$\sigma_j = -1$ means site j is vacant. This model has a bulk phase transition at $\beta_c = 0.221\,655$ (Ref. 30). For $T < T_c$ there may be a first-order interface between a predominantly $\sigma_j = +1$ phase and a predominantly $\sigma_j = -1$ phase. The ECS is a cube at $T = 0$. For $0 < T < T_R$ all interface orientations are expected to be stable.³¹ At $T = 0$ the (100) facet consists of a plane of bonds between spins of opposite sign. As T increases, fluctuations are excited as spins flip in the bulk (gas atoms and vacancies) and on the interface (adsorbed and desorbed atoms). This is most easily visualized not in terms of broken bonds but in terms of their dual-lattice plaquettes. Each plaquette corresponds to a unit of interfacial area and costs energy 2 (i.e., $2J$).

In order to study a step on a (100) interface, we need to make appropriate changes in the Hamiltonian (16). Consider the Ising system as filling a box of volume V and height L_z in which (100) lattice planes of area A are stacked at $z = \pm\frac{1}{2}, \pm\frac{3}{2}, \pm\frac{5}{2}, \dots$. To eliminate wall energies and to enforce a (100) interface, connect the box periodically in the x and y directions and antiperiodically in the z direction. The (100) interface can be stabilized at $z = 0$ by applying an infinitesimal external symmetry breaking field, as described, for example, by Weeks *et al.*¹³ The ground state of this interface is a plane of plaquettes at $z = 0$. Let the coordinates of the dual-lattice sites in this plane be given by two integers (n_x, n_y) . We now modify the lattice by piercing it with two screw dislocations of Burgers vector $-\hat{z}$ at $(0,0)$ and $+\hat{z}$ at (N,M) . This forces a step into the interface running from $(0,0)$ to (N,M) at average angle $\theta = \arccos(N/L)$ with the length $L \equiv (N^2 + M^2)^{1/2}$. Between the dislocations, this step divides the interface into an upper and a lower terrace. We chose to enforce the step in this manner (rather than by boundary conditions) for combinatorial reasons. We envision the ground state of the interface with this step to be planar everywhere except for the “tear” consisting of the $|N| + |M| \equiv K$ extra plaquettes constituting the shortest possible step from $(0,0)$ to (N,M) . This state has degeneracy $d_0(N,M) = \binom{K}{|M|}$, because the step may stride $|N|$ times in the x direction and $|M|$ times in the y direction in any order [Fig. 3(a)]. As T increases, atoms adsorb and desorb on the facet and the step will begin to lengthen and to develop overhangs [Fig. 3(b)]. The total free energy of this system will have contributions scaling like V from the bulk, like A from the (100) interface, like L from the step, and like L_z from the screw dislocations, plus end effects of order unity from the regions where the step terminates. Since we wish to extract the step free energy, we must also subtract the screw-dislocation contribution in addition to the bulk and surface terms already subtracted in Eqs. (8b) and (12). It turns out that the screw dislocations do not contribute to the orders considered in our calculation. Thus, we absorb them, for notational convenience, in the bulk free-energy term, i.e., $f_b \rightarrow f_b + 2(L_z/V)f_{\text{screw}}$, where they can henceforth be ignored.

In the canonical ensemble, the macroscopic orientation of the step is fixed by fixing N and M . As a consequence, plaquettes can only be excited in pairs so that \mathcal{H} has eigenvalues $E_n = 4n$ where n is one half the number of pla-

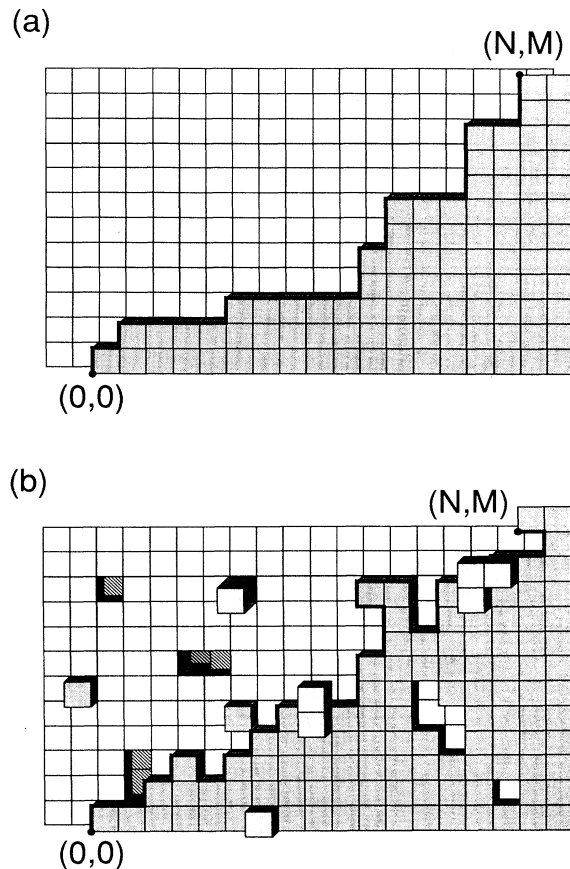


FIG. 3. Typical step configurations of the simple-cubic Ising (100) interface: (a) $T = 0$, (b) $T > 0$. The “bare” step is, by convention, a non-self-intersecting line lying in the plane as indicated by the bold line.

quettes. The lowest excited state corresponds to adding two plaquettes to the step. The canonical low- T expansion variable is, therefore, $v \equiv e^{-4\beta}$, and the expansion of the canonical partition functions becomes

$$\text{Tre}^{-\beta\mathcal{H}_{z,\theta}} = d_0 e^{-2\beta(A+K)} \left[1 + \sum_{n=1}^{\infty} g_n(N,M; A; V) v^n \right], \quad (17)$$

where $d_0 g_n$ is the degeneracy of the n th excited state.

In the grand canonical ensemble, step orientations are summed over by summing over M at fixed N . The ground state is then nondegenerate and corresponds to a straight step of N plaquettes from $(0,0)$ to $(N, M = 0)$. Because M is free, plaquettes can be excited one at a time with the lowest excited state corresponding to the two steps of $N + 1$ plaquettes from $(0,0)$ to $(N, M = \pm 1)$. The expansion variable is now $w \equiv e^{-2\beta} = \sqrt{v}$. At order w^n the step can terminate at the $n + 1$ positions $[N, M(n, m)]$, where $M(n, m) = n - 2m$ with $m \in \{0, 1, 2, \dots, n\}$. For a step terminating at M , the

field contribution to the Hamiltonian is $x\hat{x} \cdot \int_{\mathcal{L}} d\mathcal{L} \hat{\mathbf{z}} = -xM$ and the grand partition function becomes

$$\sum_{\theta} \text{Tr} \exp \left[-\beta \left[\mathcal{H}_{2,\theta} - x\hat{x} \cdot \int_{\mathcal{L}} d\mathcal{L} \hat{\mathbf{z}} \right] \right] = e^{-2\beta(A+N)} \left[1 + \sum_{n=1}^{\infty} \tilde{g}_n(x) w^n \right], \quad (18)$$

with

$$\tilde{g}_n(x) = \sum'_{M=n(\text{mod}2)} \binom{K}{M} g_{(n-M)/2}(N, M; A; V) \times [2 \cosh(\beta x M) - \delta_{M,0}], \quad (19)$$

where the prime indicates that the sum is over even (odd) M if n is even (odd), and we have taken advantage of the symmetry, $g_n(N, M) = g_n(N, -M)$. Low- T expansions for $\Gamma(\hat{\mathbf{z}})$ and f_b take the form³²

$$\Gamma(\hat{\mathbf{z}}) = 2 - T \sum_{j=2}^{\infty} \Gamma_j v^j \quad (20)$$

and

$$f_b = -T \sum_{j=3}^{\infty} f_b v^j. \quad (21)$$

Low- T expansions of $\gamma(\theta)$ and $y(x)$ are obtained by substituting (17) and (18) [and also (20) and (21)] into (8b) and (12), respectively, to obtain

$$\gamma(\theta) = 2(c+s) - T[(c+s)\ln(c+s) - c \ln c - s \ln s] - T \lim_{L \rightarrow \infty} \frac{1}{L} \sum_{j=1}^{\infty} (\gamma_j - A \Gamma_j - V f_b) v^j \quad (22)$$

and

$$y(x) = 2 - T \lim_{N \rightarrow \infty} \frac{1}{N} \left[\sum_{j=1}^{\infty} y_j w^j - \sum_{i=2}^{\infty} (A \Gamma_i + V f_b) w^{2i} \right], \quad (23)$$

where $c \equiv |\cos\theta|$, $s \equiv |\sin\theta|$. $\sum_{j=1}^{\infty} \gamma_j v^j$ and $\sum_{j=1}^{\infty} y_j v^j$ are the series expansions of $\ln(1 + \sum_{n=1}^{\infty} g_n v^n)$ and $\ln(1 + \sum_{n=1}^{\infty} \tilde{g}_n w^n)$, respectively. Note that, if the limit of Eq. (23) is to exist, then y_{odd} cannot contain any A - or V -dependent terms. Equation (22) shows that, at $T=0$, $\gamma(\theta)$ has cusps at $\theta=0$ and symmetry equivalent angles. It follows from the symmetry of the lattice that, at finite temperature, $\partial\gamma(\theta)/\partial\theta=0$ at $\theta=\pi/4$ and $\theta=0$. Since all step orientations are stable, Eq. (9) then implies that, conveniently, $\gamma(0)=y(0)$ and $\gamma(\pi/4)=\sqrt{2}y(x=y)$.

To calculate the degeneracies g_n , it is most useful to develop a diagrammatic notation. To this end, we distinguish three classes of excitations [see Fig. 3(b)]. These are (1) single-layer adsorptions and desorptions on the upper and lower terraces but not overhanging the step, (2) multilayer excitations and overhangs, and (3) bulk excitations (bubbles), i.e., excitations not topologically connected to the main sheet of plaquettes. Class 2 may be further subdivided into configurations not containing

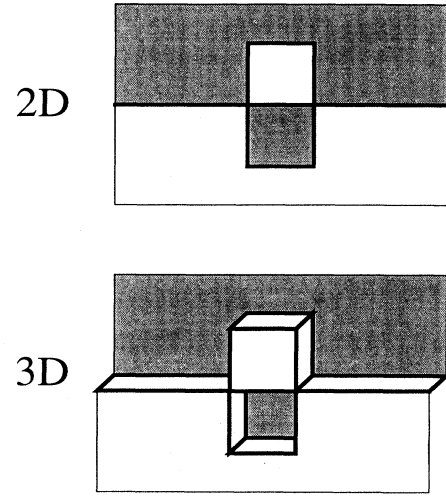


FIG. 4. This figure illustrates that the step cannot be chosen as a single non-self-intersecting line without ambiguity. For the configuration shown, that ambiguity arises in the same way for the 2D and 3D Ising models. If we let white be “up” and shaded be “down,” this configuration could be considered to be either a step with a downward indentation and a white disconnected excitation or a step with an upward indentation and a shaded disconnected excitation. At each order considered in this paper, the number of ambiguous 2D configurations equaled the number of ambiguous 3D configurations (Ref. 34).

overhangs, so-called solid-on-solid (SOS) configurations and non-SOS configurations. If we include only class 1 and class 2 SOS configurations, we obtain the expansion for the corresponding SOS model.¹⁴ For combinatorial convenience, it is our convention here to take the step itself (the “bare” step) to be a single, non-self-intersecting line lying in the plane. Since this line cannot generally be chosen without ambiguity in the presence of additional excitations (see Fig. 4), summing over all possible distinct lines (of some given length) in accordance with this convention leads to an overcounting which must be compensated. The method described below turns out to handle this problem automatically, at least to the orders calculated. We shall comment further on this point at the end of this section. For class 1 configurations, we adopt the diagrammatic notation shown in Fig. 5. Class 2 and 3 excitations will be denoted by self-explanatory pictures (Fig. 6).

Each diagram contains the “bare” step plus a number (possibly zero) of disconnected parts denoting additional excitations. These disconnected parts contain contributions to facet and bulk free energies in addition to the step free energy. The contribution to the step free energy results from the fact that the presence of the step reduces the number of configurations available to the disconnected excitations. Since a given state of \mathcal{H} corresponds to a fixed number of plaquettes, we can describe this interaction as being due to two mechanisms: First, disconnected diagrams abutting the step are not allowed because this

would annihilate plaquettes and, secondly, disconnected diagrams straddling the step are not allowed as this would create plaquettes. We may, therefore, write for the class 1 diagram $\mathcal{S} \sim \mathcal{D}$

$$\mathcal{S} \sim \mathcal{D} = \mathcal{S} \times \mathcal{D} - (\mathcal{S} \sim \mathcal{D})_d, \tag{24}$$

where $(\mathcal{S} \sim \mathcal{D})_d$ denotes the number of \mathcal{D} configurations disallowed in the presence of the step \mathcal{S} . For singly disconnected diagrams we have

$$(\mathcal{S} \sim \mathcal{D})_d = (\mathcal{S} \sim \mathcal{D})_A + (\mathcal{S} \sim \mathcal{D})_S, \tag{25}$$

where $(\mathcal{S} \sim \mathcal{D})_A$ denotes the number of abutting and $(\mathcal{S} \sim \mathcal{D})_S$ the number of straddling configurations. Multiply disconnected diagrams are more complicated but the same general principles apply.

If we were to allow only desorptions on the upper terrace level and adsorptions on the lower, interface configurations would be isomorphic to those of the 2D Ising model with an interface between “up” and “down” phases in lieu of the step. For this model the interfacial free energy $\Gamma_{2D}(\theta)$ and the ECS $y_{2D}(x)$ are known exactly.¹⁷⁻¹⁹ Although the symmetry of \mathcal{H} between adsorptions and desorptions destroys this isomorphism, we can still take advantage of the exact 2D solution to simplify the full 3D combinatorics. Note that class 1 diagrams can equally well be used in the expansion of $\Gamma_{2D}(\theta)$ and $y_{2D}(x)$, if we ignore the fact that they are to represent both adsorptions and desorptions. In 2D, the nature of the “interaction” between disconnected parts and the step remains unchanged from 3D (dual-lattice bonds replacing dual-lattice plaquettes), so Eqs. (24) and (25) hold also for the 2D interpretation of the diagrams. For singly disconnected diagrams $(\mathcal{S} \sim \mathcal{D})_{3DS} = 2(\mathcal{S} \sim \mathcal{D})_{2DS}$, as both adsorptions and desorptions can straddle the step. However, \mathcal{S} and $(\mathcal{S} \sim \mathcal{D})_A$ have the same value, whether interpreted as 2D or 3D configurations, because adsorptions (desorptions) are allowed to abut the step on the upper (lower) terrace. This allows us to shift the necessity for doing the explicit combinatorics of many 2D configurations up by several orders from where they first occur by writing

generic symbol	diagram	definition
\mathcal{S}_0		$\frac{1}{d_0} \times$ [number of configurations of a step of $ M + N +n$ plaquettes whose ends are fixed at (0,0)]
\mathcal{S}_n		and (N, M) ; $d_0 \equiv \binom{ M + N }{ M }$
\mathcal{D}^1		number of configurations available to ad/desorptions of the shape indicated
\mathcal{D}^2		
$\mathcal{S} \sim \mathcal{D}$		$\frac{1}{d_0} \times$ (number of disconnected configurations possible in the presence of the step indicated)

FIG. 5. Definitions for class 1 diagrams.

#	DIAGRAM	WEIGHT
I		$\frac{ N (N +1)}{ M +1} + \frac{ M (M +1)}{ N +1}$
II		$2(K - \frac{ N M }{K})$
III		$\left\{ \frac{1}{2} \left[\frac{ N (N +1)}{(M +1)(M +2)} (K+ M +N^2+2)+ N M \right] + 2 \frac{K+1}{ M +1} + K - \frac{ N M }{K} - 2 \right\} + \{N \leftrightarrow M\}$
IV		$\left\{ \frac{2 N (N^2+ N +1)}{ M +1} + K + N M \right\} + \{N \leftrightarrow M\}$
V		$4K - \frac{4 N M }{K} + 2$

Δg_3 :

CLASS 1		
#	DIAGRAM	WEIGHT
1		$-K$

Δg_4 :

CLASS 1		
#	DIAGRAM	WEIGHT
2		$-(K+2) \times (I)$
3		$-(K+1)$
4		$-2K$
5		$-2K - (II)$
6	Δ	$(II) + K$

CLASS 2		
#	DIAGRAM	WEIGHT
7		$-(II)$
8		$2K$

FIG. 6. A list of the diagrams which had to be evaluated explicitly to obtain the correction terms to the 2D Ising model at the orders indicated. Each of the class 2 and 3 diagrams shown has another version in which gas and solid sites are symmetrically interchanged. All these configurations are, of course, included in the weights given. Only V - and A -independent terms are given; as in the text, $K \equiv |M| + |N|$. The subscript A indicates that the number of forbidden *abutting* configurations is to be counted. The subscript 2DS means that the number of forbidden *straddling* configurations of the diagram, interpreted as a 2D diagram, is to be calculated. $\Delta(\text{diagram})$ denotes the difference between the 3D and 2D interpretations of the diagram. The notation $\{N \leftrightarrow M\}$ means that the previous term with N and M interchanged is to be added.

Δg_5 :

CLASS 1		
#	DIAGRAM	WEIGHT
9		$-(K+4) \times (\text{III})$
10		$-(K+3) \times (\text{I})$
11		$-2(K+2) \times (\text{I}) + 2 \frac{N^2+M^2}{K}$
12		$-2(K+2) \times (\text{I}) - (\text{IV})$
13		$(\text{IV}) + (K+2) \times (\text{I})$
14		$2K - 10 \times (\text{I}) + 2 \times (\text{V}) + (K+6) \times (\text{II})$
15		$-3K$
16		$-12K + 2 NM \frac{3K-4}{K(K-1)}$
17		$-3K-4$
18		$-8(K+1) - 2 \times (\text{II})$
19		$-2K - 2 \times (\text{II})$
20		$-2K - 2 \times (\text{II})$

CLASS 2		
#	DIAGRAM	WEIGHT
21		$-(\text{IV})$
22		$2(K+2) \times (\text{I})$
23		$8 \frac{ NM }{K} - 12K - 4$
24		$2K$
25		$2 \times (\text{II})$
26		$2 \frac{ NM }{K}$
27		$2 \frac{ NM }{K}$

CLASS 3		
#	DIAGRAM	WEIGHT
28		$-2K$
29		$-K$

FIG. 6. (Continued).

$$\gamma(\theta) = \Gamma_{2D}(\theta) - T \lim_{L \rightarrow \infty} \frac{1}{L} \sum_{j=1}^{\infty} [(\gamma_j - \gamma_{2D_j}) - A(\Gamma_j - f_{2D_{b_j}}) - Vf_b] v^j \quad (26)$$

$$\equiv \Gamma_{2D}(\theta) - T \sum_{j=1}^{\infty} \left[\lim_{L \rightarrow \infty} \frac{\Delta \gamma_j}{L} \right] v^j \equiv \Gamma_{2D}(\theta) - T \sum_{j=1}^{\infty} b_j v^j \quad (27)$$

and

$$y(x) = y_{2D}(x) - T \lim_{L \rightarrow \infty} \frac{1}{L} \left[\sum_{j=1}^{\infty} (y_j - y_{2D_j}) w^j - \sum_{i=2}^{\infty} [A(\Gamma_i - f_{2D_{b_i}}) + Vf_{b_i}] w^{2i} \right] \quad (28)$$

$$\equiv y_{2D}(\theta) - T \sum_{j=1}^{\infty} \left[\lim_{L \rightarrow \infty} \frac{\Delta y_j}{L} \right] w^j \equiv y_{2D}(\theta) - T \sum_{j=1}^{\infty} \tilde{b}_j w^j. \quad (29)$$

In these equations γ_{2D_j} and y_{2D_j} are the 2D versions of γ_i and y_i , respectively, i.e., they are the terms in Eqs. (22) and (23) arising from the 2D interpretation of class 1 diagrams. f_{2D_b} is the 2D bulk free energy for the 2D Ising model. The effect of this rearrangement is that many

terms cancel in the outermost brackets of (26) and (28), so that the number of diagrammatic terms corresponding to $\Delta \gamma_i$ and Δy_i that remain to be evaluated is significantly reduced (at least at low orders). This is a tremendous simplification, as the order-by-order calculation of \mathcal{S} and

TABLE I. Summary of the low- T expansion of the step free energy $\gamma(\theta)$.

$\gamma(\theta) = \Gamma_{2D}(\theta) - T \sum_{n=3}^{\infty} b_n e^{-4\beta n}$ $c \equiv \cos\theta , s \equiv \sin\theta $				
n	b_n	3D Ising $\theta = \pi/4$	SOS $\theta = \frac{\pi}{4}$	
3	$-(c+s)$	$-\sqrt{2}$	$-(c+s)$	
4	$2\frac{cs}{c+s} - 4(c+s) - 2\left(\frac{c^2}{s} + \frac{s^2}{c}\right)$	$-\frac{11}{2}\sqrt{2}$	$2\frac{cs}{c+s} - 6(c+s) - 2\left(\frac{c^2}{s} + \frac{s^2}{c}\right)$	
5	$2\left(\frac{c^4}{s^3} + \frac{s^4}{c^3}\right) + \frac{2}{c+s}(7cs-1)$ $-27(c+s) - 8\left(\frac{c^2}{s} + \frac{s^2}{c}\right)$	$-\frac{61}{2}\sqrt{2}$	$2\left(\frac{c^4}{s^3} + \frac{s^4}{c^3}\right) + \frac{2}{c+s}(7cs-1)$ $-30(c+s) - 12\left(\frac{c^2}{s} + \frac{s^2}{c}\right)$	

$(\mathcal{S} \sim \mathcal{D})_A$ diagrams is exceedingly tedious. Also, all terms involving A and V vanish, as is necessary if the thermodynamic limit $L \rightarrow \infty$ is to exist. Because these terms cancel, the $\Delta\gamma_i$ and Δy_i can be expressed entirely in terms of the A - and V -independent parts of g_i and g_{2D_i} . If a_i , Δg_i , \bar{a}_i , and $\Delta \bar{g}_i$ denote the A - and V -independent parts of g_{2D_i} , $(g_i - g_{2D_i})$, \bar{g}_{2D_i} , and $(\bar{g}_i - \bar{g}_{2D_i})$, respectively, we can, therefore, simply write

$$\sum_{j=1}^{\infty} \Delta\gamma_j v^j = \ln \left[1 + \sum_{i=1}^{\infty} (a_i + \Delta g_i) v^i \right] - \ln \left[1 + \sum_{i=1}^{\infty} a_i v^i \right] \quad (30)$$

and

$$\sum_{j=1}^{\infty} \Delta y_j w^j = \ln \left[1 + \sum_{i=1}^{\infty} (\bar{a}_i + \Delta \bar{g}_i) w^i \right] - \ln \left[1 + \sum_{i=1}^{\infty} \bar{a}_i w^i \right]. \quad (31)$$

It is crucial here that a_i , Δg_i , \bar{a}_i , and $\Delta \bar{g}_i$ contain not only the terms of order L^1 , but also those of order L^0 , since the latter get multiplied by order L^1 terms at higher order in the expansion of the logarithms. The nonvanishing a 's and Δg 's needed in (30) for the calculation of the $\Delta\gamma_i$ to order 5, inclusively, have the diagrammatic expansions

$$\begin{aligned} a_1 &= (\text{I}), \\ a_2 &= (\text{III}) - (\text{II}), \\ \Delta g_3 &= (1), \\ \Delta g_4 &= (2) + (3) + (4) + (5) + (6) + (7) + (8), \\ \Delta g_5 &= \sum_{D=9}^{29} (D), \end{aligned} \quad (32)$$

where the numbers in parentheses label diagrams listed (with their numerical equivalents) in Fig. 6. The corrections Δy_i can now be evaluated to eleventh order *without*

calculating additional diagrams. The expansions of the necessary nonvanishing \bar{a}_i and $\Delta \bar{g}_i$ are simply obtained by appropriate substitution into Eq. (19) (put $g = a$ to evaluate \bar{a} and $g = \Delta g$ to evaluate $\Delta \bar{g}$).³³

To the orders calculated here, the method of expansion described above solves the problems associated with the ambiguity of defining the step as a single, non-self-intersecting line (Fig. 4). We find that, with consistent use of that definition, diagrams conspire such that the number of overcounted configurations is the same for the 2D model as it is for the 3D model, so that they cancel in the calculation of the Δg_i (Ref. 34).

IV. RESULTS AND DISCUSSION

The results of our expansions are summarized in Tables I and II. The series for $\Gamma_{2D}(\theta)$ and $y(x)_{2D}$ are given in Tables III and IV (see also Appendix A). Let $\gamma(\theta, N)$ and $y(x, N)$ denote the series for $\gamma(\theta)$ and $y(x)$ summed to order N , inclusively. Figure 7 shows the be-

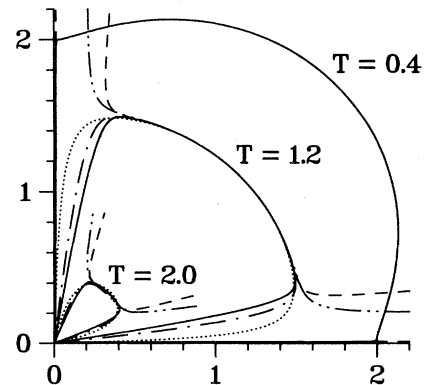


FIG. 7. Polar plots of the low-temperature series of $\gamma(\theta)$ at the temperatures indicated. The different line styles indicate the order to which the series was summed: the dotted line is the first, the dash-double dotted line is the second, the dash-dotted line is the third, the dashed line is the fourth, and the solid line is the fifth order. At $T=0.4$ the divergent region about $\theta=0$ and $\pi/2$ is still very narrow and barely resolved in the figure.

TABLE II. Summary of the low- T expansion of the equilibrium facet shape $y(x)$.
$$y(x) = y_{2D}(x) - T \sum_{n=6}^{\infty} \bar{b}_n(x) e^{-2\beta n}$$

$$\chi \equiv \cosh(\beta x)$$

n	3D Ising			SOS	
	$\bar{b}_n(x)$	$x=0$	$\bar{b}_n(x)$	$x=0$	
6	-1	-1	-1	-1	-1
7	-2χ	-2	-2χ	-2	-2
8	$-4\chi^2$	-4	$-4\chi^2 - 2$	-6	-6
9	$-8\chi^3 + 2\chi$	-6	$-8\chi^3 - 2\chi$	-10	-10
10	$-16\chi^4 - 16\chi^2 + 3$	-29	$-16\chi^4 - 24\chi^2 + 8$	-32	-32
11	$-32\chi^5 - 72\chi^3 + 68\chi$	-36	$-32\chi^5 - 88\chi^3 + 74\chi$	-46	-46

expansion as a function of θ . $\gamma(\theta, N)$ diverges about its $T=0$ cusps at $\theta=0$ and converges best at $\theta=\pi/4$ (and their symmetry equivalent angles). Interestingly, the angular radius of convergence decreases with increasing T and presumably vanishes at T_R , reflecting the singular nature of the step free energy, which is expected to go to zero in Kosterlitz-Thouless fashion like^{3,35}

$$\gamma(\theta) \rightarrow B e^{-C/\sqrt{T_R - T}} \quad \text{as } T \rightarrow T_R^-, \quad (33)$$

where B and C are constants. On the other hand, $y(x, N)$ converges best at $x=0$ ($\theta=0$), with a radius of convergence in x which also appears to vanish as $T \rightarrow T_R$. Figure 8 shows $y(x, 11)$ as a function of x and the Legendre transform of $\gamma(\theta, 5)$, both normalized to the crystal diameter [cf. Eq. (15)]. At low temperatures the grand canonical series nicely fills in the part of the facet shape not obtainable from the canonical series. Figure 9 shows a plot of $\gamma(\theta, N)$ versus T in the symmetry directions $\theta=\pi/4$ and $\theta=0$. These series appear to converge to the asymptotic form (33) (see also Fig. 10) by developing minima which move with increasing order toward the T axis from below. This behavior of the series is consistent with that of the BCRSOS model^{6,7} which, for $\theta=\pi/4$, is given to order v^{40} in Appendix B.

To investigate the asymptotic properties of our series, standard Padé and ratio methods³⁶ cannot be used directly because the singularity of Eq. (33) is an essential singularity. Since there is no obvious way of circumventing this problem, we use alternate methods, motivated mainly from a study of the exact solution of the BCRSOS model.^{6,7} The low- T series for $\gamma(\pi/4)$ of the BCRSOS model (see Appendix B) is an alternating series: Order v is negative, orders v^2 to v^{10} are positive, orders v^{11} to v^{35} are negative, and so on. The number of consecutive terms of like sign presumably increases with increasing order. For $T \lesssim 0.85T_R$, the convergence of this series is dominated by the first sequence of positive terms, i.e., the terms of order v^n with $n \in \{k, \dots, l\}$, where $k=2$ and $l=10$ here. Let a_n denote the coefficient of v^n . It turns out that the ratio $r_n \equiv a_n/a_{n-1}$, decreases with n for $n \in \{k+1, \dots, l\} \equiv \mathcal{P}$. Hence, if T is sufficiently low such that $vr_m < 1$, it follows that $vr_n < 1$ for $n \geq m$ ($n, m \in \mathcal{P}$) and, therefore, the series $\sum_{n=m}^l a_n v^n$ is bounded by the geometric series $xa_m v^m \sum_{j=0}^{l-m-1} x^j \equiv xa_m v^m S(l, m)$, where $x \equiv vr_m$. Thus, if $m \ll l$, a reasonable estimate for $\sum_{n=m}^{\infty} a_n v^n$ is $a_m v^m x S(\infty, m) = a_m v^m x / (1-x)$.

We shall assume that the generic form of the complete series for the step free energy of the SC Ising model is similar to that of the corresponding series of the

TABLE III. Coefficients of the low- T expansion of the 2D-Ising interfacial free energy $\Gamma_{2D}(\theta)$.
$$\Gamma_{2D}(\theta) = 2 - T \sum_{n=0}^{\infty} b_{2D_n}(\theta) e^{-4\beta n}$$

n	$b_{2D_n}(\theta)$	$c \equiv \cos\theta , s \equiv \sin\theta $
0	$(c+s)\ln(c+s) - c \ln c - s \ln s$	
1	$(c^3 + s^3)/(cs)$	
2	$[-3(c^7 + s^7) + 2(s^5 + c^5)]/(2c^3 s^3)$	
3	$[9(c^{11} + s^{11}) - 10(c^9 + s^9) + 3(c^7 + s^7)]/(3c^5 s^5)$	
4	$[-31(c^{15} + s^{15}) + 44(c^{13} + s^{13}) - 22(c^{11} + s^{11}) + 4(c^9 + s^9)]/(4c^7 s^7)$	
5	$[121(c^{19} + s^{19}) - 204(c^{17} + s^{17}) + 132(c^{15} + s^{15}) - 40(c^{13} + s^{13}) + 5(c^{11} + s^{11})]/(5c^9 s^9)$	
6	$[-515(c^{23} + s^{23}) + 1006(c^{21} + s^{21}) - 786(c^{19} + s^{19}) + 312(c^{17} + s^{17}) - 65(c^{15} + s^{15}) + 6(c^{13} + s^{13})]/(6c^{11} s^{11})$	

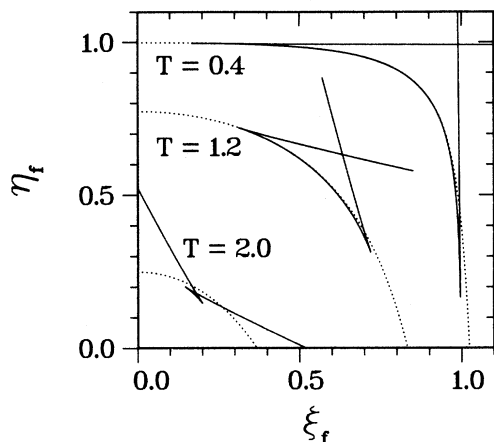


FIG. 8. The facet shape at different temperatures, normalized to the center-of-crystal to center-of-facet distance as obtained from the eleventh-order series for $y(x)$ (dotted curve) and the Legendre transform of the fifth-order series for $\gamma(\theta)$ (solid curve). The nonphysical parts of the Legendre transform are the result of the divergences of the series for $\gamma(\theta)$ (see Fig. 7). Note that the dotted curves are not symmetric under reflection about $x=y$. This effect is a consequence of distinguishing the x and y axes in the grand canonical expansion and disappears at infinite order. Because of the convergence properties of the series, the best numerical estimates of the facet shape at finite order are obtained for $\theta \in [\pi/4, \pi/2]$.

BCRSOS model. In order to estimate the error made in truncating the series after order N , let us assume further that the grand canonical series cannot converge significantly better than the canonical series, so that we can restrict our analysis to $\theta = \pi/4$. For the Ising and SOS models, the foregoing paragraph then implies that it is reasonable to expect the series for the error $\Delta_N \equiv \gamma(\pi/4) - \gamma(\pi/4, N)$, for $N \geq 4$, to be bounded by a

geometric series, so that

$$\Delta_N \leq \bar{\Delta}_N \equiv -Tv^N(b_N + \frac{\sqrt{2}}{N})x/(1-x),$$

provided $0 < x < 1$, where

$$x = v \left[b_N + \frac{\sqrt{2}}{N} \right] / \left[b_{N-1} + \frac{\sqrt{2}}{N-1} \right]$$

is the ratio of the N th to the $(N-1)$ st term of $\gamma(\pi/4, N)$. While it is only clear that this must be so at sufficiently low T , we shall assume that $\bar{\Delta}_N$ gives a reasonable error estimate for fractional errors $\bar{\Delta}_5/[\gamma(\pi/4, 5) + \bar{\Delta}_5]$ as high as $\sim 10\%$. For $N=5$ we find that the fractional error is less than (0.1%, 1%, 5%, 10%) for $T \leq (1.72, 1.92, 2.04, 2.09)$; for $N=4$ these temperatures are (1.61, 1.78, 1.87, 1.90). For the SOS model the corresponding estimates are for $N=5$, $T \leq (1.73, 1.93, 2.07, 2.12)$ and for $N=4$, $T \leq (1.51, 1.62, 1.66, 1.67)$.

If we take the fractional error in approximating $\gamma(\theta)$ by $\Gamma_{2D}(\theta)$ to be $1 - \Gamma_{2D}(\theta)/[\gamma(\pi/4, 5) + \bar{\Delta}_5]$ we find it to be less than 1% for $T < 1.79$ (less than 0.1% for $T < 1.51$). Below $T = 1.79$ the order v^4 and v^5 non-SOS contributions are less than 0.08 and 0.03%, respectively, so that bubbles and overhangs are unimportant in this temperature range. Above $T = 1.79$, the facet-shape anisotropy, as approximated by $[\gamma(\pi/4, 5) - \gamma(0, 11)]/\gamma(0, 11)$, is less than 4×10^{-3} for both the Ising and SOS models. At $T = 1.79$, the normalized facet radius $\rho_f = 0.4$. It follows that, in the region of temperature where the facet has experimentally significant anisotropy (i.e., for $T \lesssim 1.8$), the facet shape is essentially given by the 2D Ising ECS with the convergent corrections calculated in Sec. II.

TABLE IV. Coefficients of the low- T expansion of the 2D-Ising equilibrium crystal shape $y_{2D}(\theta)$.

n	$\bar{b}_{2D_n}(x)$	$\chi \equiv \cosh(\beta x)$
1	2χ	
2	$2\chi^2 - 2$	
3	$\frac{8}{3}\chi^3 - 2\chi$	
4	$4\chi^4 - 4$	
5	$\frac{32}{5}\chi^5 + 8\chi^3 - 14\chi$	
6	$\frac{32}{3}\chi^6 + 32\chi^4 - 46\chi^2 + \frac{10}{3}$	
7	$\frac{128}{7}\chi^7 + 96\chi^5 - 128\chi^3 + 14\chi$	
8	$32\chi^8 + 256\chi^6 - 304\chi^4 + 16$	
9	$\frac{512}{9}\chi^9 + 640\chi^7 - 608\chi^5 - \frac{704}{3}\chi^3 + 146\chi$	
10	$\frac{512}{5}\chi^{10} + 1536\chi^8 - 928\chi^6 - 1504\chi^4 + 818\chi^2 - \frac{122}{5}$	
11	$\frac{2048}{11}\chi^{11} + 3584\chi^9 - 512\chi^7 - 6560\chi^5 + 3448\chi^3 - 146\chi$	
12	$\frac{1024}{3}\chi^{12} + 8192\chi^{10} + 3584\chi^8 - 23\,552\chi^6 + 11\,556\chi^4 - \frac{364}{3}$	

In the temperature range $1.8 \lesssim T \lesssim 2.1$, T is high enough for the series to differ significantly from the 2D Ising series but low enough for us still to have some confidence that the series have converged. Assuming that in this region $\gamma(\pi/4, 5)$ and $y(0, 11)$ are already well approximated by their asymptotic form (33), one may hope to extract the critical parameters B , C , and T_R .

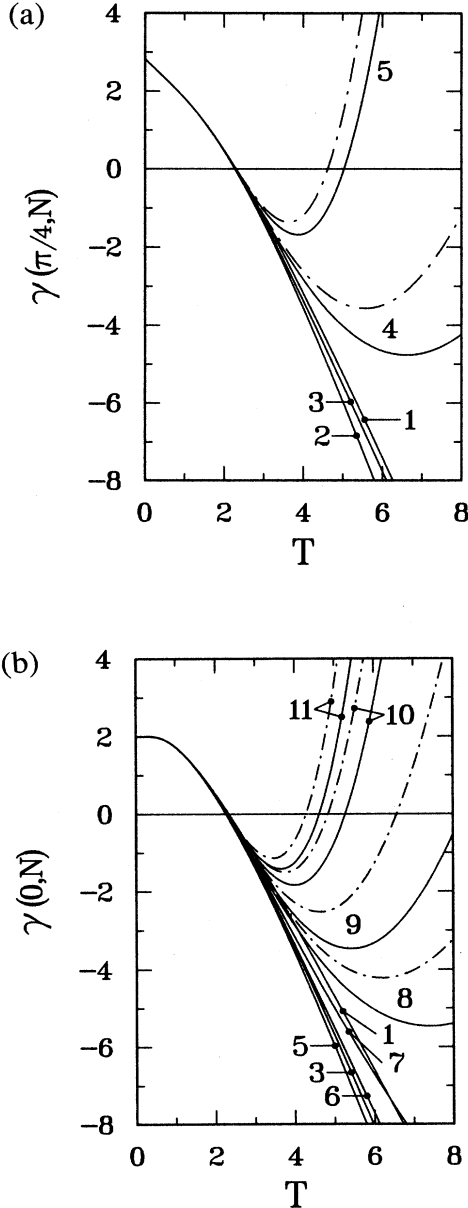


FIG. 9. (a) The canonical series $\gamma(\pi/4, N)$ for the step free energy and (b) the grand canonical series $y(0, N)$ for the facet shape, summed to the orders N indicated, as a function of temperature. Conveniently, $\sqrt{2}y(x=y) = \gamma(\pi/4)$ and $y(0) = \gamma(0)$ as discussed after Eq. (23). The solid curves are the Ising result; the dash-dotted curves are the SOS result.

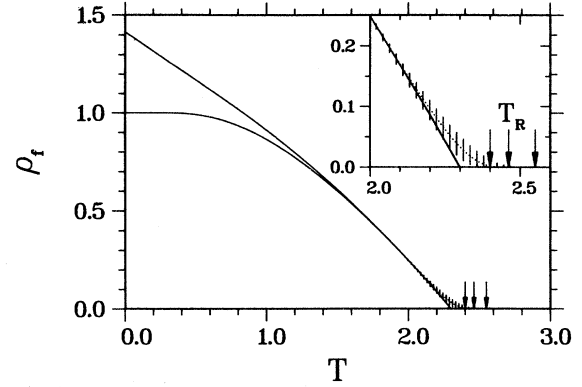


FIG. 10. The normalized facet radius ρ_f in the symmetry directions as a function of temperature. The lower (upper) solid curve is calculated from the canonical (grand canonical) series summed to fifth (eleventh) order at $\theta=0$ ($\theta=\pi/4$). The dotted curve is an extrapolation into the critical region, as described in the text. The error bars indicate the uncertainty associated with that extrapolation. The middle arrow indicates the T_R associated with the dotted curve. The arrow on the left-hand side (right-hand side) indicates the lower (upper) limit of T_R , as estimated by Adler (Ref. 16) and corresponds to the lower (upper) limits of the error bars shown.

Indeed, plots of

$$C(T) \equiv -2(T_R - T)^{3/2} \partial \ln \gamma(\theta, N) / \partial T$$

and

$$B(T) \equiv \gamma(\theta, N) \exp[C(T) / \sqrt{T_R - T}]$$

versus T for various values of T_R , at $\theta=\pi/4$ and 0, show a plateau for $T_R = T_{P(\text{plateau})} \approx 2.46$ over the temperature range $1.8 \lesssim T \lesssim 2.0$. The failure of the plateau to extend beyond $T=2.0$ is consistent with the convergence estimates above. The functions $B(T)$ and $C(T)$ [which would be constants if the series were exactly equal to (33)] have qualitatively the same shape: For $T_R > T_P$, they increase monotonically over the temperature range of interest; for $T_R < T_P$, the plateau deepens into a minimum which becomes deeper and more narrow with decreasing T_R . Guided again by the BCRSOS model and the fact that we observe no significant change in the plateau parameters from order $N=4$ to order $N=5$, we take the plateau parameters to be the critical parameters. To extract these parameters numerically, we performed a least-squares fit of the functional form (33) to $[\gamma(\pi/4, 5) + y(0, 11)]/2$ over a temperature interval of width 0.2 centered at T^* with fitting parameters B , C , T_R , and T^* . For the Ising model we obtain $B = 9.7 \pm 1.0$, $C = 2.05 \pm 0.15$, and $T_R = 2.46 \pm 0.02$ with $T^* = 1.9$. For the SOS model $B = 10.3 \pm 1.5$, $C = 2.13 \pm 0.15$, and $T_R = 2.48 \pm 0.03$ with $T^* = 1.9$. The uncertainties quoted are associated with the fit and do not necessarily represent an estimate of how close these numbers might be to the true critical values. The roughening tempera-

tures obtained in this way are consistent with $T_R(\text{Ising})=2.475\pm 0.075$ and $T_R(\text{SOS})=2.54\pm 0.07$, as obtained by Adler,¹⁶ for the Ising model, all the critical parameters are consistent with $B=9.84\pm 2.0$, $C=2.12\pm 0.13$, and $T_R=2.44\pm 0.09$, as obtained from Monte Carlo data for $\gamma(0)$.¹² Figure 10 shows the T dependence of the normalized facet diameter of the Ising model, extrapolated all the way to T_R using our fit to Eq. (33). The lower (upper) limit of the error bars shown there correspond to fits obtained over the interval $1.905\leq T\leq 1.955$ with T_R constrained to be the lower (upper) limit of Adler's estimates for T_R . We emphasize that we do not recommend the methods of this paper if one is interested in T_R only (and not, for example, in the amplitudes B and C also). In such cases, the series methods of Weeks *et al.*,^{13,14} with their well-understood asymptotic analysis,¹⁶ are probably more efficient. Our calculation, on the other hand, is the only one so far to address the anisotropic step free energy and the shape and size of facets.

It is interesting to examine the assumption that the series are already in the asymptotic regime over the temperature range $1.8\lesssim T\lesssim 2.1$ in the context of the Monte Carlo simulations of Mon *et al.*¹² While their data, extrapolated to infinite system size, shows (33) to hold over the entire temperature range $1.8<T<T_R$, they fall below the 2D Ising value by about 10% at $T=1.8$, where our expansion implies that the 2D Ising result is a lower bound. In principle, this discrepancy could be due to large negative coefficients at higher orders of our expansion; however, in light of the preceding discussion, this is unlikely. A more likely source of error, as pointed out by Mon *et al.* in Ref. 12, is the finite-size-scaling analysis of the Monte Carlo data, performed with only three data points at each value of T . The fact that our critical parameters agree with those of Mon *et al.* in spite of these problems is probably attributable to the sensitive dependence of $\gamma(\theta)$ on the precise numerical values of the critical parameters.

V. CONCLUSIONS

We have shown how to calculate step free energies and the corresponding equilibrium facet shapes in low-temperature expansion. The combinatorics involved is significantly reduced by structuring these expansions as perturbation series about the interfacial properties of the 2D Ising model. The two expansions are related by a Legendre transform and can be thought of as canonical and grand canonical representations of the same physics. The grand canonical form of the expansion gives the facet shape where it is not accessible from the canonical expansion of the step free energy.

At temperatures where the facet has experimentally significant anisotropy, the facet shape is essentially given by the 2D Ising ECS normalized to the facet's surface free energy, with convergent corrections displayed in Tables I and II of this paper. Corrections to the 2D Ising result due to additional (non-2D) SOS, overhanging, and bubble configurations enter at orders $e^{-12\beta J}$, $e^{-16\beta J}$, and

$e^{-20\beta J}$, respectively. These corrections are less than 1% for $0<T<1.79\approx 0.72T_R$ and less than 0.1% for $0<T<1.51\approx 0.61T_R$. In this temperature range, overhangs and bubbles are unimportant. At higher temperatures the facet shape is nearly circular, with a normalized facet radius of less than 0.4 and anisotropies of less than 0.1%. Numerical extrapolations into the asymptotic critical temperature region of the step free energy yield roughening amplitudes consistent with recent Monte Carlo data.¹² The effect of non-2D-Ising configurations is to raise the roughening temperature from T_c (2D Ising) to the true T_R (an increase of $\sim 9\%$) and to build in the proper Kosterlitz-Thouless roughening singularity.

The facet-shape information provided by Figs. 8 and 10 is potentially useful in analyzing experimental data from any real crystals which may be modeled by the nearest-neighbor SC Ising model, but for which the effective nearest-neighbor coupling is unknown. For example, T_R is often difficult to measure by direct observation of the vanishing of the facet, either because the facet edge cannot be located precisely³⁷ (and/or is very sensitive to dynamical effects) or because the roughening transition is preempted by bulk melting. In such situations, it may be feasible to measure the facet diameter in one of the symmetry directions at a lower temperature T_{exp} . The corresponding reduced temperature T can be read off Fig. 10, from which the effective nearest-neighbor coupling is determined as $J=k_B T_{\text{exp}}/T$. The roughening temperature is then given by (from Ref. 16)

$$T_{R_{\text{exp}}} = (T_{\text{exp}}/T)(2.475\pm 0.075) .$$

In nature most crystals are unfortunately not simple cubic, and next-nearest-neighbor interactions cannot always be neglected. As long as interactions remain nearest neighbor, generalization is straightforward. If next-nearest-neighbor forces must be accounted for, the nature of the problem changes drastically. The energy of a configuration will now depend not only on the number of plaquettes but also on the number of corners. This makes the combinatorics very difficult and completely different in character from what we have had to deal with here. It is clear that, in any case, it will be useful to expand about a 2D model describing the central layer containing the step. An interesting open question is whether the step free energy is rigorously bounded from below by the interfacial free energy of that 2D model and, if so, under what conditions.

ACKNOWLEDGMENTS

We thank T. Templeton for showing us how to use the minimization software MINUIT. One of us (M.H.) would like to thank Simon Fraser University for financial support in the form of a graduate scholarship. This work was funded in part by the Natural Sciences and Engineering Research Council of Canada.

**APPENDIX A: SERIES
FOR THE 2D ISING MODEL**

The interface free energy per unit length and the ECS of the 2D Ising model are given in their most convenient form in Refs. (17) and (19), respectively, as

$$\beta\Gamma_{2D}(\theta) = |\cos\theta|\operatorname{arcsinh}(\alpha|\cos\theta|) + |\sin\theta|\operatorname{arcsinh}(\alpha|\sin\theta|) \quad (\text{A1})$$

and

$$|y_{2D}(x)| = T \operatorname{arccosh} \left[\frac{1}{h} - \cosh(\beta x) \right], \quad (\text{A2})$$

where

$$\alpha \equiv \frac{1}{h} \left[\frac{1-4h^2}{1+(\sin^2 2\theta + 4h^2 \cos^2 2\theta)^{1/2}} \right]^{1/2} \quad (\text{A3})$$

and

$$h \equiv \frac{\sinh 2\beta}{\cosh^2 2\beta}. \quad (\text{A4})$$

Expanding (A1) in powers of $v \equiv e^{-4\beta}$ and (A2) in powers of $w \equiv e^{-2\beta}$, we obtain (with the aid of an algebraic ma-

nipulation computer program) the series displayed in Tables III and IV. In the symmetry directions these expressions simplify to

$$\begin{aligned} \Gamma_{2D}(0) = y_{2D}(0) &= 2 + T \ln(\tanh\beta) \\ &= 2 - 2T \sum_{n_{\text{odd}}=1}^{\infty} \frac{w^n}{n} \end{aligned} \quad (\text{A5})$$

and

$$\begin{aligned} \frac{1}{\sqrt{2}}\Gamma_{2D}(\pi/4) = y_{2D}(x = y_{2D}) &= T \ln(\sinh 2\beta) \\ &= 2 - T \left[\ln 2 + \sum_{n=1}^{\infty} \frac{v^n}{n} \right]. \end{aligned} \quad (\text{A6})$$

**APPENDIX B: SERIES FOR $\gamma(\pi/4)$
OF THE BCRSOS MODEL**

Reference 7 gives a closed form series for the BCRSOS facet shape in terms of implicitly defined functions. Reexpanding this series (with $J \rightarrow 2J$ to make contact with the energy scale of this paper) in powers of $v = \exp(-4\beta)$ we obtain, aided by the algebraic manipulation program REDUCE,

$$\begin{aligned} \frac{1}{\sqrt{2}}\gamma\left(\frac{\pi}{4}\right)(\text{BCRSOS}) &= 2 + T(-\ln 2 - v + \frac{1}{2}v^2 + \frac{14}{3}v^3 + \frac{65}{4}v^4 + \frac{234}{5}v^5 + \frac{371}{3}v^6 + \frac{2148}{7}v^7 + \frac{5665}{8}v^8 + \frac{13010}{9}v^9 \\ &+ \frac{10823}{5}v^{10} - \frac{6172}{11}v^{11} - \frac{150053}{6}v^{12} - \frac{1993668}{13}v^{13} - \frac{5083256}{7}v^{14} - \frac{15445312}{5}v^{15} - \frac{198297247}{16}v^{16} \\ &- \frac{814643486}{17}v^{17} - \frac{1625206543}{9}v^{18} - \frac{12681689860}{19}v^{19} - \frac{4858460157}{2}v^{20} - 8726304516v^{21} \\ &- \frac{340811734532}{11}v^{22} - \frac{2502599042576}{23}v^{23} - \frac{4536558436405}{12}v^{24} - \frac{32478199348916}{25}v^{25} \\ &- \frac{57358896324242}{13}v^{26} - \frac{399349718315896}{27}v^{27} - \frac{341863037952600}{7}v^{28} - \frac{4591877224341056}{29}v^{29} \\ &- \frac{7525021925258524}{15}v^{30} - \frac{47780502385670032}{31}v^{31} - \frac{145024421300144799}{32}v^{32} \\ &- \frac{410388042705413374}{33}v^{33} - \frac{510842904954910389}{17}v^{34} - \frac{1840425563886041612}{35}v^{35} \\ &+ \frac{356819183917550041}{18}v^{36} + \frac{31642674797949425588}{37}v^{37} + \frac{11414142063730282438}{19}v^{38} \\ &+ \frac{422991335163343500056}{13}v^{39} + \frac{630708193372567078915}{4}v^{40} + \dots \end{aligned}$$

¹C. Rottman and M. Wortis, Phys. Rep. **103**, 59 (1984).

²R. K. P. Zia, *Proceedings of the Twenty-Sixth Scottish Universities Summer School in Physics on Statistical and Particle Physics: Common Problems and Techniques, Edinburgh, 1983*, edited by K. C. Bowler and A. J. McKane (Scottish Universities Summer School in Physics, Edinburgh, 1984), pp. 247–301.

³H. van Beijeren and I. Nolden, *Topics in Current Physics*, edited by W. Schommers and P. von Blanckenhagen (Springer, Berlin, 1987), Vol. 43, pp. 259–300.

⁴M. Wortis, *Chemistry and Physics of Solid Surfaces*, edited by R. Vanselow (Springer-Verlag, Berlin, 1988), Vol. VII, pp. 367–405.

⁵W. K. Burton, N. Cabrera, and F. C. Frank, Philos. Trans. R.

Soc. London, Ser. A **243**, 299 (1951).

⁶H. van Beijeren, Phys. Rev. Lett. **38**, 993 (1977).

⁷C. Jayaprakash, W. F. Saam, and S. Teitel, Phys. Rev. Lett. **50**, 2017 (1983).

⁸C. Jayaprakash and W. F. Saam, Phys. Rev. B **30**, 3916 (1984).

⁹S. T. Chui and J. D. Weeks, Phys. Rev. B **14**, 4978 (1976).

¹⁰D. A. Huse, W. van Saarloos, and J. D. Weeks, Phys. Rev. B **32**, 233 (1985).

¹¹N. Akutsu and Y. Akutsu, J. Phys. Soc. Jpn. **56**, 1443 (1987).

¹²K. K. Mon, S. Wansleben, D. P. Landau, and K. Binder, Phys. Rev. Lett. **60**, 708 (1988); see also, Phys. Rev. B **39**, 7089 (1989).

¹³J. D. Weeks, G. H. Gilmer, and H. J. Leamy, Phys. Rev. Lett. **31**, 549 (1973).

- ¹⁴H. J. Leamy, G. H. Gilmer, and K. A. Jackson, *Surface Physics of Crystalline Materials* (Academic, New York, 1975), p. 169.
- ¹⁵L. J. Shaw and M. E. Fisher, *Phys. Rev. A* **39**, 2189 (1989).
- ¹⁶J. Adler, *Phys. Rev. B* **36**, 2473 (1987).
- ¹⁷C. Rottman and M. Wortis, *Phys. Rev. B* **24**, 6274 (1981).
- ¹⁸J. E. Avron, H. van Beijeren, L. S. Schulman, and R. K. P. Zia, *J. Phys. A* **15**, L81 (1982).
- ¹⁹R. K. P. Zia and J. E. Avron, *Phys. Rev. B* **25**, 2042 (1982).
- ²⁰For a more general discussion from the point of view of equilibrium crystal shapes see *Surface Physics of Crystalline Materials*, Ref. 14; a pedagogical discussion is given by R. B. Griffiths, *Phase Transitions in Surface Films*, edited by J. G. Dash and J. Ruvalds (Plenum, New York, 1980), pp. 1–27.
- ²¹Instead of thinking of the interface as resulting from some modification of the Hamiltonian, a point of view which we adopt here primarily for notational convenience, we could equally well have enforced an interface by imposing appropriate boundary conditions. For further discussion on this point and its subtleties see the rigorous discussion by D. B. Abraham, *Phase Transitions and Critical Phenomena*, edited by C. Domb and J. L. Lebowitz (Academic, New York, 1986), Vol. 10, pp. 2–69.
- ²²G. Wulff, *Z. Kristallogr. Mineral* **34**, 449 (1901).
- ²³C. Herring, *Phys. Rev.* **82**, 87 (1951).
- ²⁴A. F. Andreev, *Zh. Eksp. Teor. Fiz.* **80**, 2042 (1981) [*Sov. Phys.—JETP* **53**, 1063 (1982)].
- ²⁵N. Cabrera, *Surf. Sci.* **2**, 320 (1964).
- ²⁶Consider, for example, the Ising model. Draw a closed curve C on its boundary, dividing it into two parts of approximately equal area. Demanding all spins to be up on one part and down on the other will force an interface to span C . If C deviates from lying in a plane by distances comparable to the system size, the resulting interface will not be macroscopically planar. Since we assume here that the Wulff construction holds, such configurations carry no statistical weight, for, if they did, the ECS could not be constructed from the surface tensions of macroscopically planar interfaces alone. Thus, even through the grand canonical ensemble contains systems with all possible curves C , we can, in practice, sum over only those with curves C admitting macroscopically planar configurations, i.e., $\{\hat{m}\} \rightarrow \hat{m}$.
- ²⁷ $v=3$ for short-ranged forces due to entropic step-step repulsions. This means that the ECS curves away from the facet edge with exponent $\frac{3}{2}$; see V. L. Pokrovsky and A. L. Talapov, *Phys. Rev. Lett.* **42**, 65 (1979); C. Jayaprakash, C. Rottman, and W. F. Saam, *Phys. Rev. B* **30**, 6549 (1984), and references therein.
- ²⁸We take the azimuthal angle θ to be measured clockwise from the y axis here.
- ²⁹From the analytical statement of the full 3D Wulff construction in Cartesian form, this was shown by Akutsu and Akutsu in Ref. 11.
- ³⁰G. S. Pawley, R. H. Swendsen, D. J. Wallace, and K. G. Wilson, *Phys. Rev. B* **29**, 4030 (1984).
- ³¹C. Rottman and M. Wortis, *Phys. Rev. B* **29**, 328 (1984).
- ³²The expansion for the (100) surface tension of the simple-cubic Ising model was calculated by J. D. Weeks, G. H. Gilmer, and H. J. Leamy (Ref. 13). The series was not published in the original literature and was only recently quoted in Ref. 15 as $\Gamma(\hat{z})(\text{Ising}) = 2 - T(2v^2 + 2v^3 + 10v^4 + 16v^5 + \frac{242}{3}v^6 + 150v^7 + 734v^8 + \frac{4334}{3}v^9 + \dots)$. For completeness we quote their SOS result which is published in Ref. 14: $\Gamma(\hat{z})(\text{SOS}) = 2 - T(2v^2 + 4v^3 + 10v^4 + 24v^5 + \frac{194}{3}v^6 + 172v^7 + 452v^8 + \frac{3185}{3}v^9 + \dots)$.
- ³³The calculation of the diagrams appearing in the grand canonical expansion is easier (at least at low orders) than the calculation of the canonical diagrams, in the sense that the former, unlike the latter, need not be calculated for general M . This fact may be useful to push our calculation to higher order to get more information in the critical region. Since the facet is essentially isotropic there, the fact that the grand canonical series converges best in only one symmetry direction ($\theta=0$) is not a serious limitation.
- ³⁴This cancellation is transparent for simple diagrams such as those shown in Fig. 3. We have checked it to the orders considered in this paper. Whether it persists to all orders is unclear.
- ³⁵J. P. von der Eerden and H. J. F. Knops, *Phys. Lett. A* **66**, 334 (1978); R. H. Swendsen, *Phys. Rev. B* **17**, 3710 (1978).
- ³⁶See, for example, D. S. Gaunt and A. J. Guttmann, *Phase Transitions and Critical Phenomena*, edited by C. Domb and M. S. Green (Academic, New York, 1974), Vol. 3, pp. 181–243.
- ³⁷See, for example, F. Gallet, P. Nozières, S. Balibar, and E. Rolley, *Europhys. Lett.* **2**, 701 (1986).

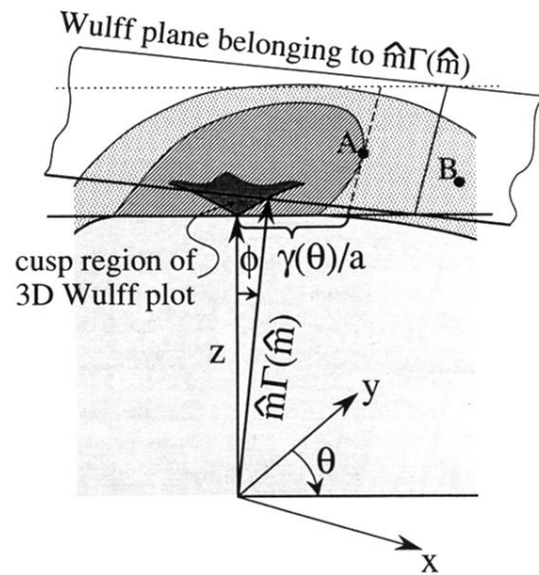


FIG. 1. Perspective view of a fixed- θ cut through the ECS and its Wulff plot as described in the text. The Wulff plane shown is tangent to the ECS at point B in the rounded or rough region of the ECS. In the limit as $\phi \rightarrow 0$ ($\hat{m} \rightarrow \hat{z}$) this plane intersects the facet plane, which is the Wulff plane of the cusp, along a line (dashed) which is at perpendicular distance $\gamma(\theta)/a$ from the cusp and tangent to the facet at point A . The facet shape is obtained as the 2D Wulff construction of $\gamma(\theta)/a$.

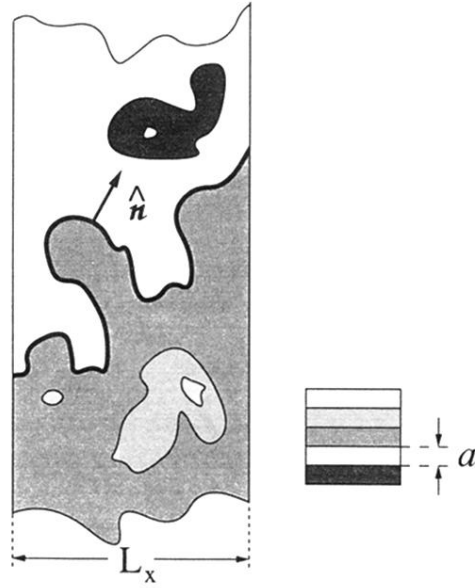


FIG. 2. A strip of vicinal surface projected onto the xy plane. The shading represents lattice planes of spacing a at different levels. The strip contains a “bare” step \mathcal{L} (bold line) and excitations on the terraces to either side of the step (closed curves). \hat{n} is the 2D microscopic normal to the step in the xy plane. The field contribution to the grand canonical Hamiltonian $\eta \cdot \int_{\mathcal{S}} (\Delta m_x, \Delta m_y) d\mathcal{S} = a\eta \cdot \int_{\text{all curves}} d\mathcal{L} \hat{n}$ vanishes around closed curves and therefore couples only to the “bare” step.

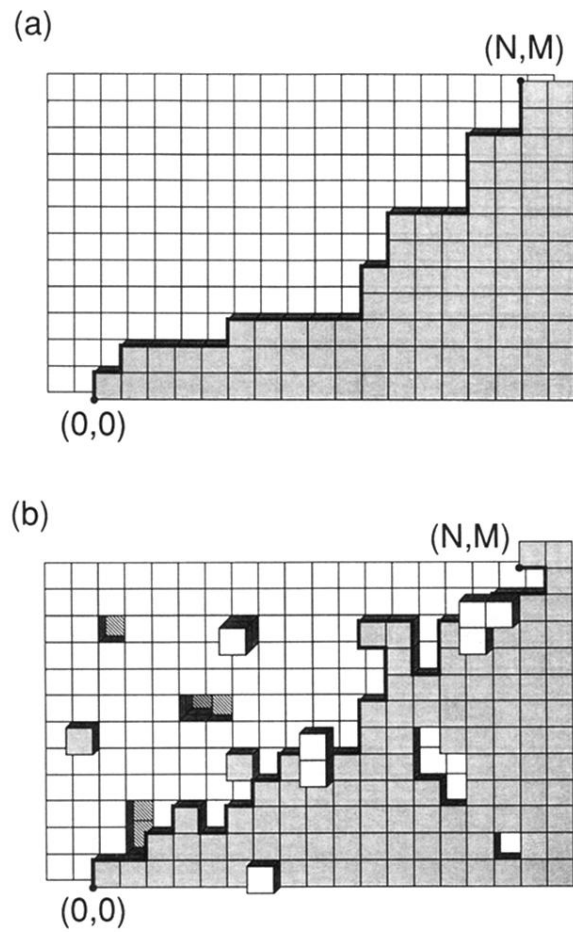


FIG. 3. Typical step configurations of the simple-cubic Ising (100) interface: (a) $T=0$, (b) $T>0$. The “bare” step is, by our convention, a non-self-intersecting line lying in the plane as indicated by the bold line.

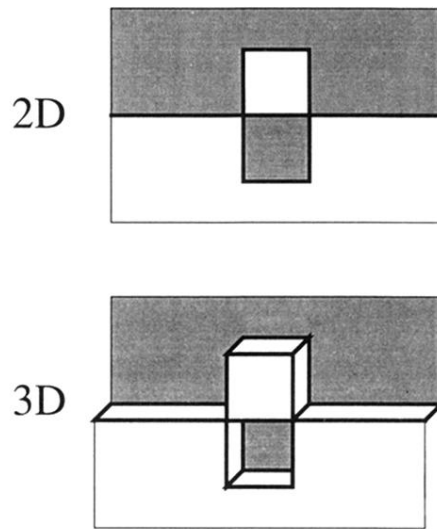


FIG. 4. This figure illustrates that the step cannot be chosen as a single non-self-intersecting line without ambiguity. For the configuration shown, that ambiguity arises in the same way for the 2D and 3D Ising models. If we let white be “up” and shaded be “down,” this configuration could be considered to be either a step with a downward indentation and a white disconnected excitation or a step with an upward indentation and a shaded disconnected excitation. At each order considered in this paper, the number of ambiguous 2D configurations equaled the number of ambiguous 3D configurations (Ref. 34).